

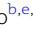



# Nonequilibrium noise as a probe of pair-tunneling transport in the BCS–BEC crossover

 Hiroyuki Tajima <sup>a,\*</sup>, Daigo Oue <sup>b,c,d</sup>, Mamoru Matsuo <sup>b,e,f,g</sup> and Takeo Kato <sup>h</sup>
<sup>a</sup>Department of Physics, Graduate School of Science, The University of Tokyo, Tokyo 113-0033, Japan

<sup>b</sup>Kavli Institute for Theoretical Sciences, University of Chinese Academy of Sciences, Beijing 100190, China

<sup>c</sup>Instituto Superior Técnico, University of Lisbon, Lisboa 1049-001, Portugal

<sup>d</sup>The Blackett Laboratory, Department of Physics, Imperial College London, Prince Consort Road, Kensington, London SW7 2AZ, UK

<sup>e</sup>CAS Center for Excellence in Topological Quantum Computation, University of Chinese Academy of Sciences, Beijing 100190, China

<sup>f</sup>Advanced Science Research Center, Japan Atomic Energy Agency, Tokai 319-1195, Japan

<sup>g</sup>RIKEN Center for Emergent Matter Science (CEMS), Wako, Saitama 351-0198, Japan

<sup>h</sup>The Institute for Solid State Physics, The University of Tokyo, Kashiwa 277-8581, Japan

 \*To whom correspondence should be addressed: Email: [hiroyuki.tajima@phys.s.u-tokyo.ac.jp](mailto:hiroyuki.tajima@phys.s.u-tokyo.ac.jp)

Edited By: Derek Abbott

## Abstract

The detection of elementary carriers in transport phenomena is one of the most important keys to understand nontrivial properties of strongly correlated quantum matter. Here, we propose a method to identify the tunneling current carrier in strongly interacting fermions from nonequilibrium noise in the Bardeen–Cooper–Schrieffer to Bose–Einstein condensate crossover. The noise-to-current ratio, the Fano factor, can be a crucial probe for the current carrier. Bringing strongly correlated fermions into contact with a dilute reservoir produces a tunneling current in between. The associated Fano factor increases from one to two as the interaction becomes stronger, reflecting the fact that the dominant conduction channel changes from the quasiparticle tunneling to the pair tunneling.

**Keywords:** transport, nonequilibrium noise, strongly interacting fermions, BCS–BEC crossover

## Significance Statement

The anatomy of the elementary transport carriers involving strong correlations has been a long-standing issue in the fields of cold atoms as well as superconductors. We show that the Fano factor, the ratio between a current and its nonequilibrium noise, reflects information on anomalous pair-tunneling transport in strongly correlated superfluids and superconductors. The Fano factor changes from 1 to 2, according to whether the quasiparticle or the pair tunneling is dominant, and hence can be a direct probe for the nontrivial pair-tunneling current. Our result can be tested in cold atomic and condensed matter experiments.

Transport phenomena have contributed to the development of the fundamental physics in previous centuries. Various unconventional phenomena such as superfluidity and superconductivity were observed using transport measurements. However, clarifying the microscopic mechanism of the transport phenomena in strongly correlated systems remains challenging because of their complexities such as strong interactions, lattice geometries, as well as multiple degrees of freedom.

Recently, an ultracold atomic system has been regarded as a quantum simulator for strongly correlated many-body systems such as unconventional superconductors and nuclear systems, owing to its controllability of physical parameters (e.g. interparticle interactions and lattice structures) and its cleanliness (1, 2). In particular, state-of-the-art experiments for tunneling current have been conducted in strongly interacting Fermi gases (3–8). Moreover, thermoelectric transport has been demonstrated experimentally in an ultracold Fermi gas (9). A quantum point

contact has also been implemented for atomic superfluid junctions (10). These experiments motivate us to study tunneling transport associated with the Josephson effect and Cooper-pair tunneling in the superfluid phase of the Bardeen–Cooper–Schrieffer (BCS) to Bose–Einstein condensate (BEC) crossover (11–19). Such a direction are recently referred to as *atomtronics* (20).

One crucial problem is to understand how strong correlations affect the conduction mechanism, which is necessary for future development of quantum-transport technology. Recently, several theoretical efforts have been paid to understand an anomalous tunneling current induced by pairing fluctuations in the normal phase (21–24), as observed in experiments (3–8). It is anticipated that such anomalous pair-tunneling currents can be induced by the nonlinear tunneling processes (21), tunneling of a closed-channel molecule (22), and the proximity effect associated with two-body interactions (25). However, regardless of

**Competing Interest:** The authors declare no competing interest.

**Received:** October 1, 2022. **Revised:** December 15, 2022. **Accepted:** January 23, 2023

© The Author(s) 2023. Published by Oxford University Press on behalf of National Academy of Sciences. This is an Open Access article distributed under the terms of the Creative Commons Attribution License (<https://creativecommons.org/licenses/by/4.0/>), which permits unrestricted reuse, distribution, and reproduction in any medium, provided the original work is properly cited.

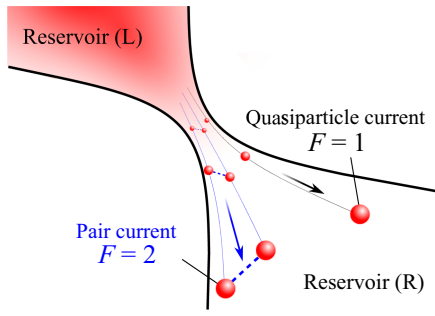


**Fig. 1.** Strongly interacting quantum gases (reservoirs L and R) with a large chemical potential bias in between. The Fano factor  $F$  can be regarded as an indicator of the current carrier, i.e. quasiparticle current ( $F = 1$ ) and the pair current ( $F = 2$ ).

these different origins, the existence of the pair-tunneling current itself is still an important pending problem because it is difficult to distinguish quasiparticle- and pair-tunneling currents experimentally. In this sense, it is worth exploring clear evidence for anomalous pair currents in a strongly interacting Fermi gas.

For this purpose, measuring the Fano factor is promising, which is defined by a current and the associated nonequilibrium noise (26, 27). The Fano factor in the large-biased setup reflects the effective charge per elementary transport process regardless of system's detail. The most fascinating example is the detection of fractional charges in fractional quantum Hall systems (28, 29). The Fano factor has been used to determine the effective charge (or spin) in various physical systems such as superconductors (30, 31), Kondo quantum dots (32, 33), and magnetic junctions (34–37). Once the Fano factor is measured in strongly interacting Fermi gases, the existence of the pair-tunneling current will be revealed in an unbiased way.

In this study, we show that the Fano factor  $F$  can be used as a probe for the current carrier in the BCS–BEC crossover. Fig. 1 shows a schematic setup of the large-biased system. Using the many-body T-matrix approach (TMA) (38, 39), we numerically calculate the current and nonequilibrium noise within the Schwinger–Keldysh approach in the two-terminal tunneling junction under a large bias. We reveal how the Fano factor  $F$  changes in a strongly interacting regime, thereby reflecting the change of the dominant carrier. In particular, the change of  $F$  is a crucial evidence for the pair-tunneling current. Our result can be tested by cold-atom experiments for which the noise measurement has been theoretically proposed (40). Moreover, the Fano factor provides direct information of pair-fluctuation effects rather than other measurements such as spin susceptibility and photoemission spectra previously studied in this field (41). The current noise measurement can also be used to identify the carriers of the BCS–BEC crossover in condensed matter systems such as FeSe semimetal (42–45), lithium-intercalated layered nitrides (46, 47), magic-angle twisted trilayer graphene (48), and organic superconductor (49). Moreover, the noise measurement has recently been conducted in a copper oxide heterostructure (50, 51) and disordered superconductor (52).

In the following, we take  $\hbar = k_B = 1$  and consider a unit volume.

## Tunneling current and noise

We consider the Hamiltonian  $H = H_L + H_R + H_{1T} + H_{2T}$ . The reservoir Hamiltonian  $H_{j=L,R}$  is given by

$$H_j = \sum_{\mathbf{p},\sigma} \xi_{\mathbf{p},j} c_{\mathbf{p},\sigma}^\dagger c_{\mathbf{p},\sigma} + g \sum_{\mathbf{q}} P_{\mathbf{q},j}^\dagger P_{\mathbf{q},j}, \quad (1)$$

where  $\xi_{\mathbf{p},j} = p^2/(2m) - \mu_j$  denotes the kinetic energy measured from the chemical potential  $\mu_j$  and  $c_{\mathbf{p},\sigma,j}$  denotes the annihilation operator of a Fermi atom with momentum  $\mathbf{p}$  and the pseudospin  $\sigma = \uparrow, \downarrow$ . The second term in Eq. 1 denotes the attractive interaction with a contact-type coupling  $g$ , where  $P_{\mathbf{q},j} = \sum_{\mathbf{p}} c_{-\mathbf{p}+\mathbf{q}/2,\downarrow,j} c_{\mathbf{p}+\mathbf{q}/2,\uparrow,j}$  is the pair-annihilation operator and  $g$  is related to the scattering length  $a$  as  $m/4\pi a = (1/g) + \sum_{\mathbf{p}} (m/p^2)$  (39).

The one-body tunneling Hamiltonian,

$$H_{1T} = \sum_{\mathbf{p},\mathbf{k},\sigma} [t_{\mathbf{p},\mathbf{k}} c_{\mathbf{p},\sigma,L}^\dagger c_{\mathbf{k},\sigma,R} + \text{h.c.}], \quad (2)$$

is associated with the one-body potential barrier, where  $t_{\mathbf{p},\mathbf{k}}$  denotes its coupling strength. The two-body tunneling Hamiltonian reads

$$H_{2T} = \sum_{\mathbf{q},\mathbf{q}'} [w_{\mathbf{q},\mathbf{q}'} P_{\mathbf{q},L}^\dagger P_{\mathbf{q}',R} + \text{h.c.}], \quad (3)$$

where  $w_{\mathbf{q},\mathbf{q}'}$  is the two-body coupling strength, induced by the local interaction term in Eq. 1 combined with the one-body potential barrier (25). Such two-body tunneling processes can also be obtained within the multiple one-body tunneling processes in the nonlinear regime (17, 21, 24, 53). We note that regardless of their origins, these two-body tunnelings induce the pair-tunneling current. Similar tunneling effects have also been examined in one-dimensional few-body systems (54, 55). Here, we do not go into details on the origin of the one- and two-body tunneling, but rather investigate their possible consequence in observable quantities. However, we emphasize that the two-body tunneling term is necessary to describe the molecule tunneling in the deep BEC side (and therefore the entire crossover), where the pair tunneling induced by the higher-order one-body tunneling process is suppressed due to the reduced dissociation of molecules with the large binding energy (24). In Fig. S1, we estimate the tunneling couplings in the case of delta-function-like potential barrier (19, 56) based on Ref. (25).

Using the Schwinger–Keldysh approach, we evaluate the expectation values of the current operator  $\hat{I} = i[\hat{N}_L, H]$  ( $\hat{N}_j = \sum_{\mathbf{p},\sigma} c_{\mathbf{p},\sigma}^\dagger c_{\mathbf{p},\sigma}$  denotes the density operator in the  $j$ -reservoir) in the steady state at the lowest-order tunneling couplings by a sum of the one- and two-body contributions as  $I = I_{\text{qp}} + I_{\text{pair}}$ , where each component reads (25)

$$\begin{aligned} I_{\text{qp}} &= \int_{-\infty}^{\infty} \frac{d\omega}{2\pi} \sum_{\mathbf{p},\mathbf{k},\sigma} |t_{\mathbf{k},\mathbf{p}}|^2 \mathcal{A}_{\mathbf{k},L}(\omega) \mathcal{A}_{\mathbf{p},R}(\omega) \\ &\quad \times [f_L(\omega) - f_R(\omega)], \\ I_{\text{pair}} &= 2 \int_{-\infty}^{\infty} \frac{d\omega}{2\pi} \sum_{\mathbf{q},\mathbf{q}'} |w_{\mathbf{q},\mathbf{q}'}|^2 \mathcal{B}_{\mathbf{q},L}(\omega) \mathcal{B}_{\mathbf{q}',R}(\omega) \\ &\quad \times [b_L(\omega) - b_R(\omega)]. \end{aligned} \quad (4)$$

In Eq. 4,  $\mathcal{A}_{\mathbf{k},j}(\omega)$  and  $\mathcal{B}_{\mathbf{q},j}(\omega)$  denote one- and two-particle spectral functions, respectively,  $f_j(\omega)$  and  $b_j(\omega)$  denote the Fermi and Bose distribution functions, and  $\mu_{b,j} = 2\mu_j$  denotes the bosonic-pair chemical potential in the  $j$ -reservoir. For the detection of the pair-tunneling current, it is crucial to consider the small tunneling coupling regime where the nonequilibrium noise reflects an effective particle number in tunneling process.<sup>a</sup>

We define the current noise as  $\mathcal{S}(t_1, t_2) = (1/2)\langle \hat{I}(t_1)\hat{I}(t_2) + \hat{I}(t_2)\hat{I}(t_1) \rangle$  (57–60) [see also, e.g. Ref. (36)]. For the steady-state transport with the time-translational symmetry, we assume that the

noise depends on  $t_1 - t_2$  as  $\bar{S}(t_1, t_2) \equiv \bar{S}(t_1 - t_2)$  (being independent of  $(t_1 + t_2)/2$ ). Its Fourier component reads

$$\bar{S}(\omega) = \frac{1}{\tau} \int_0^\tau dt_1 \int_0^\tau dt_2 e^{i\omega(t_1 - t_2)} \bar{S}(t_1 - t_2), \quad (5)$$

where  $\tau$  is the typical time scale for the noise measurement. Taking  $t = t_1 - t_2$  and  $\bar{S}(t) = \frac{1}{2}(\hat{I}(t)\hat{I}(0) + \hat{I}(0)\hat{I}(t))$ , we obtain the zero-frequency limit of the noise power  $S \equiv \bar{S}(\omega \rightarrow \eta)$  ( $\eta$  is an infinitesimally small number) as

$$S = \frac{1}{2} \int_{-\infty}^{\infty} dt (\hat{I}(t)\hat{I}(0) + \hat{I}(0)\hat{I}(t)), \quad (6)$$

where we considered the limit of  $\tau \rightarrow \infty$ . In this regard, we briefly note that  $\tau$  should be sufficiently longer than the transport time-scale  $\tau_0$ , where in the recent experiment  $\tau_0 = O(10^{-1})$  s is found (9). Similar to the calculation above, we can evaluate the current noise (Supplementary Material) as the sum of the two contributions:  $S = S_{\text{qp}} + S_{\text{pair}}$ , where

$$\begin{aligned} S_{\text{qp}} &= \int_{-\infty}^{\infty} \frac{d\omega}{2\pi} \sum_{\mathbf{p}, \mathbf{k}, \sigma} |t_{\mathbf{k}, \mathbf{p}}|^2 \mathcal{A}_{\mathbf{k}, \mathbf{L}}(\omega) \mathcal{A}_{\mathbf{p}, \mathbf{R}}(\omega) \\ &\quad \times [f_{\mathbf{L}}(\omega)[1 - f_{\mathbf{R}}(\omega)] + \{1 - f_{\mathbf{L}}(\omega)\}f_{\mathbf{R}}(\omega)], \\ S_{\text{pair}} &= 4 \int_{-\infty}^{\infty} \frac{d\omega}{2\pi} \sum_{\mathbf{q}, \mathbf{q}'} |w_{\mathbf{q}, \mathbf{q}'}|^2 \mathcal{B}_{\mathbf{q}, \mathbf{L}}(\omega) \mathcal{B}_{\mathbf{q}', \mathbf{R}}(\omega) \\ &\quad \times [b_{\mathbf{L}}(\omega)[1 + b_{\mathbf{R}}(\omega)] + b_{\mathbf{R}}(\omega)[1 + b_{\mathbf{L}}(\omega)]. \end{aligned} \quad (7)$$

The bias between the reservoirs is included in the distribution function and therefore Eq. 7 is valid for the case with the temperature bias (61). In the large chemical potential bias limit ( $\Delta\mu \equiv \mu_{\mathbf{L}} - \mu_{\mathbf{R}} \rightarrow \infty$ ), we can prove  $S_{\text{qp}}/I_{\text{qp}} = 1$  and  $S_{\text{pair}}/I_{\text{pair}} = 2$  without any further approximations (Supplementary Material). This motivates us to consider the Fano factor:

$$F = \frac{S}{I} = \frac{S_{\text{qp}} + S_{\text{pair}}}{I_{\text{qp}} + I_{\text{pair}}}. \quad (8)$$

The Fano factor  $F$  changes from 1 to 2, according to whether the quasiparticle or pair tunneling is dominant and hence, it is a useful probe for the current carrier. In particular, the Fano factor  $F$  becomes 1 and 2 in the BCS limit ( $a^{-1} \rightarrow -\infty$ ) and BEC limit ( $a^{-1} \rightarrow \infty$ ), respectively. Importantly, the deviation of  $F$  from 1 indicates a clear evidence of the pair-tunneling process yet to be not well understood in cold atomic systems (25). Therefore, the observation of  $F$  can be a crucial key for understanding transport phenomena in strongly interacting systems.

In this study, we consider the large bias regime (see Fig. 1) characterized by  $\mu_{\mathbf{L}} - \mu_{\mathbf{R}} \rightarrow \infty$  (Supplementary Material) (62) and the momentum-conserved tunneling processes as  $t_{\mathbf{p}, \mathbf{k}} = \mathcal{T}_1 \delta_{\mathbf{p}, \mathbf{k}}$  and  $w_{\mathbf{q}, \mathbf{q}'} = \mathcal{T}_2 \delta_{\mathbf{q}, \mathbf{q}'}$ , for simplicity. To see the qualitative behavior of  $F$ , we use the spectral functions  $\mathcal{A}_{\mathbf{k}, \mathbf{j}}(\omega) = -2 \text{Im} G_{\mathbf{k}, \mathbf{j}}(i\omega_n \rightarrow \omega - \mu_{\mathbf{j}} + i\eta)$  and  $\mathcal{B}_{\mathbf{q}, \mathbf{j}}(\omega) = -2 \text{Im} \mathcal{G}_{\mathbf{q}, \mathbf{j}}(iv_\ell \rightarrow \omega - \mu_{\mathbf{b}, \mathbf{j}} + i\eta)$  with an infinitesimal small number  $\eta$ , where thermal single- and two-particle propagators  $G_{\mathbf{k}, \mathbf{j}}(i\omega_n)$  and  $\mathcal{G}_{\mathbf{q}, \mathbf{j}}(iv_\ell)$  with fermion and boson Matsubara frequencies  $i\omega_n$  and  $iv_\ell$  are evaluated within the many-body TMA (63, 64) (see also Supplementary Material). We employ  $\eta = 10^{-2} E_{\text{F}, \mathbf{L}}$  in the numerical calculation to avoid the divergent behavior of the current associated with the momentum-conserved tunneling in the weak- and strong-coupling limits, where  $E_{\text{F}, \mathbf{L}} = (3\pi^2 N_{\mathbf{L}})^{2/3} / (2m)$  denotes the Fermi energy of the L reservoir with the number density  $N_{\mathbf{L}}$ . However, our result can be qualitatively unchanged by this treatment because the distribution functions play a key role in determining  $F$  rather than the detailed structures of tunneling junctions. Moreover,  $\mathcal{T}_2$  must be normalized to

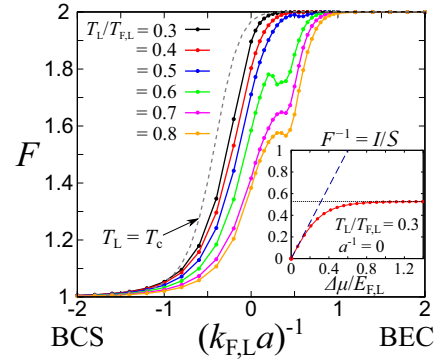


**Fig. 2.** Fano factor  $F$ , associated with tunneling transport between two reservoirs, throughout the BCS–BEC crossover for various temperatures  $T_{\mathbf{L}}$  in the reservoir L. The reservoir R is almost vacuum. The ratio between tunneling couplings is given as  $\mathcal{T}_{2,\text{ren.}}/\mathcal{T}_1 = 1$ . For comparison, we plot the result at  $T_{\mathbf{L}} = T_{\text{c}}$  (dashed curve). Note that  $T_{\text{c}}$  changes in the range of  $0.02T_{\text{F}, \mathbf{L}} \lesssim T_{\text{c}} \lesssim 0.24T_{\text{F}, \mathbf{L}}$  depending on  $(k_{\text{F}, \mathbf{L}} a)^{-1}$ . The inset shows the bias ( $\Delta\mu$ ) dependence of  $F^{-1}$  at  $T_{\mathbf{L}}/T_{\text{F}, \mathbf{L}} = 0.3$  and  $a^{-1} = 0$ . The dashed and dotted lines represent the Onsager's relation  $F^{-1}(\Delta\mu \rightarrow 0) = \Delta\mu/2T$  (Supplementary Material) and the large bias limit, respectively.

suppress the ultraviolet divergence in  $B_{\mathbf{q}, \mathbf{j}}(\omega)$ . For this purpose, we introduce the renormalized two-body tunneling coupling  $\mathcal{T}_{2,\text{ren.}} = (\Lambda^2 k_{\text{F}, \mathbf{L}} / 3\sqrt{2}\pi^2) \mathcal{T}_2$  where  $k_{\text{F}, \mathbf{L}} = \sqrt{2mE_{\text{F}, \mathbf{L}}}$  denotes the Fermi momentum. Such a divergence can also be avoided by introducing the form factor for the relative momentum  $\mathbf{p}$  in  $P_{\mathbf{q}, \mathbf{j}}$  (65). In this work, we take  $\Lambda = 100k_{\text{F}, \mathbf{L}}$  (39) in the practical calculation. This value is associated with the effective range  $r_{\text{eff}}$  as  $r_{\text{eff}} = 4/\pi\Lambda$  (39).

## Fano factor throughout the BCS–BEC crossover

Fig. 2 shows the Fano factor  $F$  as a function of the dimensionless interaction parameter  $(k_{\text{F}, \mathbf{L}} a)^{-1}$  in the entire BCS–BEC crossover regime above the superfluid critical temperature  $T_{\text{c}}$ . We considered  $\mathcal{T}_{2,\text{ren.}}/\mathcal{T}_1 = 1$ , and the reservoir R was regarded as almost vacuum ( $\mu_{\mathbf{L}} - \mu_{\mathbf{R}} \rightarrow \infty$ ) (Supplementary Material). As we showed in the inset of Fig. 2, the large-bias assumption can be justified when  $\Delta\mu$  is larger than a typical many-body scale in the reservoir (i.e.  $E_{\text{F}, \mathbf{L}}$ ). One can clearly see that  $F$  evolves from 1 to 2 with increasing the interaction strength in Fig. 2, indicating that the current carrier gradually changes from quasiparticles ( $F = 1$ ) to pairs ( $F = 2$ ). Such a behavior is universal in the sense that these asymptotic values do not depend on any details on the model parameters and structures of tunneling junctions. More explicitly, at the large bias limit, one can obtain (Supplementary Material)

$$F(\Delta\mu \rightarrow \infty) \rightarrow \frac{I_{\text{qp}} + 2I_{\text{pair}}}{I_{\text{qp}} + I_{\text{pair}}}, \quad (9)$$

where  $I_{\text{qp}}$  and  $I_{\text{pair}}$  denote the contributions of the quasiparticle and pair tunnelings, respectively. The Fano factor  $F$  approaches 1 and 2 in the quasiparticle-dominant ( $I_{\text{qp}} \gg I_{\text{pair}}$ ) and pair-dominant regimes ( $I_{\text{pair}} \gg I_{\text{qp}}$ ), respectively. Although the interaction dependence of the Fano factor  $F$  is deeply related to properties of the tunneling junctions and spectral functions of the carriers, one can find from Eq. 9 that  $F \rightarrow 1$  ( $F \rightarrow 2$ ) in the limit of  $a^{-1} \rightarrow -\infty$  ( $a^{-1} \rightarrow \infty$ ) regardless of the detailed properties of the system. Moreover,  $F = 2$  can be realized even above  $T_{\text{c}}$  because of strong interactions leading to the formation of preformed Cooper pairs in the BCS–BEC crossover. With increasing the temperature,  $F$  tends to be suppressed because thermal effects assist the

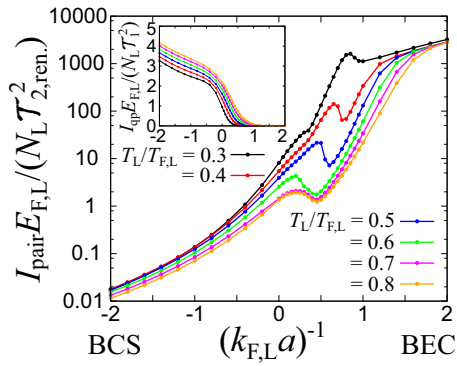


**Fig. 3.** Pair-tunneling current  $I_{\text{pair}}$  in the normal phase throughout the BCS–BEC crossover at different temperatures. The inset shows the quasiparticle current  $I_{\text{qp}}$  with the same horizontal axis  $(k_{F,L}a)^{-1}$ .

dissociation of pairs. Nevertheless, even at finite temperature,  $F$  approaches 2 with increasing the interaction because bound molecules are dominant in the deep BEC regime<sup>b</sup> where  $T_L \lesssim E_b$  [ $E_b = 1/(ma^2)$  is the two-body binding energy].

To see the detailed behavior of the Fano factor  $F$ , we plot  $I_{\text{qp}}$  and  $I_{\text{pair}}$  throughout the BCS–BEC crossover at different temperatures in Fig. 3. From the inset of Fig. 3, the quasiparticle current  $I_{\text{qp}}$  is exponentially suppressed with increasing the attractive interaction. This suppression (in particular, the rapid drop of  $I_{\text{qp}}$  at  $(k_{F,L}a)^{-1} \gtrsim -0.5$ ) is induced by the pairing fluctuation effect (39), i.e. the reduction of  $A_{\mathbf{k},L}(\omega)$  near  $|\mathbf{k}| = k_{F,L}$  and  $\omega = E_{F,L} (\simeq \mu_L)$  by the particle–hole coupling. We note that this fluctuation effects result in the pseudogap in the density of state near  $T_c$  (41). Finally,  $I_{\text{qp}}$  approaches zero in the BEC limit  $(k_{F,L}a)^{-1} \rightarrow \infty$  because of the formation of molecules with large binding energies. These results are qualitatively consistent with previous work (21, 24). On the other hand,  $I_{\text{pair}}$  drastically increases with increasing the interaction strength  $(k_{F,L}a)^{-1}$  as shown in Fig. 3. At the BCS side  $(k_{F,L}a)^{-1} < 0$  where the attraction is not strong to form a two-body bound state in vacuum, the contribution of  $I_{\text{pair}}$  can be regarded as the tunneling of the preformed Cooper pairs into the two-body continuum in the reservoir R. In the strong-coupling BEC regime  $(k_{F,L}a)^{-1} > 1$  and  $T_L/E_b \lesssim 1$ ,  $I_{\text{pair}}$  describes the tunneling transport of bound molecules across two reservoirs, because the two-body bound state exists in the reservoir R with the same coupling  $g$ . Such a tunneling current associated with weakly interacting molecular bosons becomes large due to their long lifetime and the Bose enhancement of low-energy distributions.

One can also see a dip-hump structure of  $I_{\text{pair}}$  in the intermediate regime. Here,  $\mu_L$  is close to zero and changes its sign, indicating that the dominant contribution changes from the preformed-pair transfer to the molecule-to-molecule transport across the junction. From the unitary limit  $(k_{F,L}a)^{-1} = 0$ , the preformed-pair transfer increases due to the overlap with the bound-state spectra in  $B_{\mathbf{q},R}(\omega)$  and eventually decreases because of the decrease in  $\mu_L$ . With increasing the interaction further, the inter-reservoir molecule-to-molecule transition emerges where the bound-state spectra in two reservoirs get close to each other in the energy axis  $\omega$ . Although these structures reflect the physical properties of the system, they also depend on the detailed setup of the tunneling junctions (e.g. the ratio between the tunneling couplings  $\mathcal{T}_{2,\text{ren.}}/T_1$ ) (Supplementary Material).

Fig. 4 shows the temperature dependence of the Fano factor  $F$  in the unitary limit  $(k_{F,L}a)^{-1} = 0$ . Because  $B_{\mathbf{q},R}(\omega)$  does not involve a bound molecule pole, the transfer of the preformed Cooper pairs in the reservoir L to the two-body continuum in the reservoir R

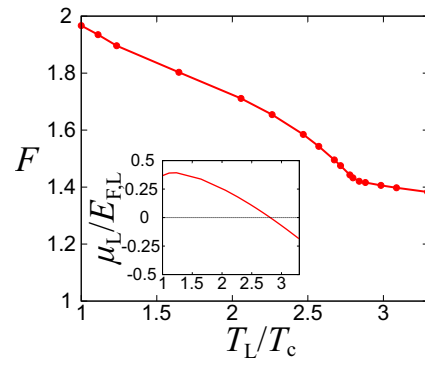


**Fig. 4.** Temperature dependence of the Fano factor  $F$  in the unitary limit [ $1/(k_{F,L}a) = 0$ ] with  $\mathcal{T}_{2,\text{ren.}}/T_1 = 1$ . The horizontal axis is taken as  $T_L/T_c$ , where  $T_c$  is the superfluid critical temperature. The inset shows the chemical potential  $\mu_L$  as a function of  $T_L/T_c$  for a given Fermi energy  $E_{F,L}$ .

can be anticipated in the unitary limit. One can see the enhancement of the Fano factor  $F$  at the low-temperature regime. In particular, the curvature of the Fano factor  $F$  is modified at  $T_L/T_c \simeq 2.8$ , where the sign of  $\mu_L$  changes from negative to positive one as the temperature decreases (see the inset of Fig. 4). Although the Fano factor depends on  $\mathcal{T}_{2,\text{ren.}}/T_1$  as shown in Fig. S2, the qualitative behavior, i.e. suppression of the pair-tunneling current due to increase of the temperature is unchanged regardless of the value of  $\mathcal{T}_{2,\text{ren.}}/T_1$ . For estimating the value of  $\mathcal{T}_{2,\text{ren.}}/T_1$  (which depends on the potential barrier and the interaction strength) in each experimental setup, see Ref. (25). In the Supplementary Material, we show that  $\mathcal{T}_{2,\text{ren.}}/T_1$  can be tuned and it is possible to realize  $\mathcal{T}_{2,\text{ren.}}/T_1 \simeq 1$  by adjusting the strength of the potential barrier as  $\mathcal{T}_{2,\text{ren.}}/T_1 \propto [1 + (V_0/E_{F,L})]^{-1} [1 + (V_0/E_{F,L})^2 (k_{F,L}\ell)^2]^{-1/2}$  for the potential barrier given by  $V = V_0\delta(x/\ell)$  perpendicular to the  $x$  axis ( $V_0$  and  $\ell$  are the strength and the characteristic length scale of the barrier). At a positive  $\mu_L$ , the pole of the preformed Cooper pairs gradually appears in  $B_{\mathbf{q},L}(\omega)$ . Thus, the behavior of the Fano factor  $F$  can be regarded as a signature of the preformed Cooper pairs. Because the preformed Cooper pairs play an important role in the pseudogap physics of ultracold Fermi gases (41), the Fano factor contributes to the further understanding of pairing pseudogaps in the BCS–BEC crossover regime. Incidentally, because TMA does not capture the self-energy shift in  $\Pi_{\mathbf{q},L}(\omega)$ , the curvature change of the Fano factor  $F$  may differ from the temperature where  $\mu_L = 0$  in actual experiments and in more sophisticated theoretical approaches (38, 39). To evaluate the spectral functions, the analytic continuation should be carefully performed in Monte Carlo simulations (66). We note that because TMA reproduces the second-order virial expansion (67), our result in the relatively high-temperature regime can give an accurate estimate of  $F$  for given tunnel couplings.

## Summary

In this study, we showed that the Fano factor (i.e. the noise-to-current ratio  $F = S/I$ ) can be a useful probe for current carriers in the BCS–BEC crossover at large-biased tunneling junctions. Using the many-body TMA, we demonstrated that the Fano factor  $F$  gradually changes from one to two as the interaction strength increases in the normal phase, indicating that the dominant current carrier changes from the quasiparticle ( $F = 1$ ) to the pair ( $F = 2$ ) along the BCS–BEC crossover. Our prediction can be tested by experiments and uncover nonequilibrium strong-coupling physics via transport measurements. While we have

focused on the large bias limit, such a situation can be achieved when the bias is larger than the many-body energy scale (i.e. Fermi energy of the dense reservoir). Furthermore, our result indicates that the noise measurement is useful for the study of the BCS–BEC crossover and pair-fluctuation effects in unconventional superconductors.

## Notes

- We note that the validity of the truncation with respect to the lowest-order tunneling coupling was confirmed in the recent experiment (7).
- Here, “BEC regime” is used for the regime where the two-body attraction is so strong that the associated superfluid state behaves like molecular BEC below  $T_c$  (38, 39). In this regard, the strongly attractive regime even above  $T_c$  is also referred as to the BEC regime for characterizing the interaction strength.
- We note that in this regime the numerical cost is large due to the overlap of Bose distribution function and sharp peaks in  $\mathcal{B}_{\mathbf{q},L,R}$ . We confirmed that the qualitative behavior is robust against the accuracy of the frequency integration.

## Supplementary material

Supplementary material is available at PNAS Nexus online.

## Funding

This work is supported in part by Grants-in-Aid for Scientific Research from JSPS (Grant Nos. JP18H05406, JP20K03831, and 22K13981). D.O. is supported by the President’s PhD Scholarships at Imperial College London, by JSPS Overseas Research Fellowship, by the Institution of Engineering and Technology (IET), and by Fundação para a Ciência e a Tecnologia and Instituto de Telecomunicações under project UIDB/50008/2020. M.M. is partially supported by the Priority Program of the Chinese Academy of Sciences (Grant No. XDB28000000). This manuscript was posted on a preprint: <https://doi.org/10.48550/arXiv.2202.03873>

## Author contributions

M.M. and T.K. designed research, H.T., D.O., M.M., and T.K. performed the calculations and wrote the manuscript.

## Data availability

All data are included in the manuscript.

## References

- Bloch I, Dalibard J, Zwerger W. 2008. Many-body physics with ultracold gases. *Rev Mod Phys.* 80:885–964.
- Chin C, Grimm R, Julienne P, Tiesinga E. 2010. Feshbach resonances in ultracold gases. *Rev Mod Phys.* 82:1225–1286.
- Krinner S, et al. 2016. Mapping out spin and particle conductances in a quantum point contact. *Proc Natl Acad Sci U S A.* 113(29):8144–8149.
- Häusler S, et al. 2017. Scanning gate microscope for cold atomic gases. *Phys Rev Lett.* 119(3):030403.
- Kwon WJ, et al. 2020. Strongly correlated superfluid order parameters from dc Josephson supercurrents. *Science.* 369(6499):84–88.
- Luick N, et al. 2020. An ideal Josephson junction in an ultracold two-dimensional Fermi gas. *Science.* 369(6499):89–91.
- Del Pace G, Kwon WJ, Zaccanti M, Roati G, Scazza F. 2021. Tunneling transport of unitary fermions across the superfluid transition. *Phys Rev Lett.* 126:055301.
- Häusler S, et al. 2021. Interaction-assisted reversal of thermopower with ultracold atoms. *Phys Rev X.* 11:021034.
- Brantut J-Pe, et al. 2013. A thermoelectric heat engine with ultracold atoms. *Science.* 342(6159):713–715.
- Husmann D, et al. 2015. Connecting strongly correlated superfluids by a quantum point contact. *Science.* 350(6267):1498–1501.
- Salasnich L, Manini N, Toigo F. 2008. Macroscopic periodic tunneling of Fermi atoms in the BCS–BEC crossover. *Phys Rev A.* 77:043609.
- Kanász-Nagy M, Glazman L, Esslinger T, Demler EA. 2016. Anomalous conductances in an ultracold quantum wire. *Phys Rev Lett.* 117:255302.
- Yao J, Liu B, Sun M, Zhai H. 2018. Controlled transport between Fermi superfluids through a quantum point contact. *Phys Rev A.* 98:041601.
- Damanet F, Mascarenhas E, Pekker D, Daley AJ. 2019. Reservoir engineering of cooper-pair-assisted transport with cold atoms. *New J Phys.* 21(11):115001.
- Zaccanti M, Zwerger W. 2019. Critical Josephson current in BCS–BEC-crossover superfluids. *Phys Rev A.* 100:063601.
- Piselli V, Simonucci S, Strinati GC. 2020. Josephson effect at finite temperature along the BCS–BEC crossover. *Phys Rev B.* 102(14):144517.
- Uchino S. 2020. Role of Nambu-Goldstone modes in the fermionic-superfluid point contact. *Phys Rev Res.* 2:023340.
- Setiawan F, Hofmann J. 2021. Analytic approach to transport in superconducting junctions with arbitrary carrier density. *Phys Rev Res.* 4:043087.
- Zhang D, Sommer AT. 2022. Transport of spin and mass at normal-superfluid interfaces in the unitary Fermi gas. *Phys Rev Res.* 4:023231.
- Amico L, et al. 2021. Roadmap on atomtronics: state of the art and perspective. *AVS Quantum Sci.* 3(3):039201.
- Uchino S, Ueda M. 2017. Anomalous transport in the superfluid fluctuation regime. *Phys Rev Lett.* 118:105303.
- Liu B, Zhai H, Zhang S. 2017. Anomalous conductance of a strongly interacting Fermi gas through a quantum point contact. *Phys Rev A.* 95:013623.
- Sekino Y, Tajima H, Uchino S. 2020. Mesoscopic spin transport between strongly interacting Fermi gases. *Phys Rev Res.* 2:023152.
- Furutani K, Ohashi Y. 2020. Strong-coupling effects on quantum transport in an ultracold Fermi gas. *J Low Temp Phys.* 201(1):49–57.
- Tajima H, Oue D, Matsuo M. 2022. Multiparticle tunneling transport at strongly correlated interfaces. *Phys Rev A.* 106:033310.
- Blanter YM, Büttiker M. 2000. Shot noise in mesoscopic conductors. *Phys Rep.* 336:1.
- Martin T. 2005. Noise in mesoscopic physics. In: Bouchiat H, Gefen Y, Guéron S, Montambaux G, Dalibard J, editors. *Nanophysics: coherence and transport, Les Houches Session LXXXI.* Chapter 5. Amsterdam: Elsevier. p. 283–359.
- de Picciotto R, et al. 1997. Direct observation of a fractional charge. *Nature.* 389:162.
- Saminadayar L, Glattli DC, Jin Y, Etienne B. 1997. Observation of the  $e/3$  fractionally charged Laughlin quasiparticle. *Phys Rev Lett.* 79:2526–2529.
- Jehl X, Sanquer M, Calemczuk R, Mailly D. 2000. Detection of doubled shot noise in short normal-metal/superconductor junctions. *Nature.* 405:50.

- 31 Kozhevnikov AA, Schoelkopf RJ, Prober DE. 2000. Observation of photon-assisted noise in a diffusive normal metal–superconductor junction. *Phys Rev Lett.* 84:3398–3401.
- 32 Zarchin O, Zaffalon M, Heiblum M, Mahalu D, Umansky V. 2008. Two-electron bunching in transport through a quantum dot induced by Kondo correlations. *Phys Rev B.* 77:241303.
- 33 Ferrier M, et al. 2016. Universality of non-equilibrium fluctuations in strongly correlated quantum liquids. *Nat Phys.* 12:230.
- 34 Kamra A, Belzig W. 2016a. Super-Poissonian shot noise of squeezed-magnon mediated spin transport. *Phys Rev Lett.* 116:146601.
- 35 Kamra A, Belzig W. 2016b. Magnon-mediated spin current noise in ferromagnet|nonmagnetic conductor hybrids. *Phys Rev B.* 94:014419.
- 36 Matsuo M, Ohnuma Y, Kato T, Maekawa S. 2018. Spin current noise of the spin Seebeck effect and spin pumping. *Phys Rev Lett.* 120:037201.
- 37 Aftergood J, Takei S. 2018. Noise in tunneling spin current across coupled quantum spin chains. *Phys Rev B.* 97:014427.
- 38 Strinati GC, Pieri P, Röpke G, Schuck P, Urban M. 2018. The BCS–BEC crossover: from ultra-cold Fermi gases to nuclear systems. *Phys Rep.* 738:1–76 (The BCS–BEC crossover: from ultra-cold Fermi gases to nuclear systems).
- 39 Ohashi Y, Tajima H, van Wyk P. 2020. BCS–BEC crossover in cold atomic and in nuclear systems. *Prog Part Nucl Phys.* 111:103739.
- 40 Uchino S, Ueda M, Brantut JP. 2018. Universal noise in continuous transport measurements of interacting fermions. *Phys Rev A.* 98:063619.
- 41 Mueller EJ. 2017. Review of pseudogaps in strongly interacting Fermi gases. *Rep Prog Phys.* 80(10):104401.
- 42 Lubashevsky Y, Lahoud E, Chashka K, Podolsky D, Kanigel A. 2012. Shallow pockets and very strong coupling superconductivity in  $\text{FeSe}_x\text{Te}_{1-x}$ . *Nat Phys.* 8(4):309–312.
- 43 Kasahara S, et al. 2014. Field-induced superconducting phase of FeSe in the BCS–BEC cross-over. *Proc Natl Acad Sci U S A.* 111(46):16309–16313.
- 44 Rinott S, et al. 2017. Tuning across the BCS–BEC crossover in the multiband superconductor  $\text{Fe}_{1+y}\text{Se}_x\text{Te}_{1-x}$ : an angle-resolved photoemission study. *Sci Adv.* 3(4):e1602372.
- 45 Hanaguri T, et al. 2019. Quantum vortex core and missing pseudogap in the multiband BCS–BEC crossover superconductor FeSe. *Phys Rev Lett.* 122(7):077001.
- 46 Nakagawa Y, et al. 2018. Gate-controlled low carrier density superconductors: toward the two-dimensional BCS–BEC crossover. *Phys Rev B.* 98:064512.
- 47 Nakagawa Y, et al. 2021. Gate-controlled BCS–BEC crossover in a two-dimensional superconductor. *Science.* 372(6538):190–195.
- 48 Park JM, Cao Y, Watanabe K, Taniguchi T, Jarillo-Herrero P. 2021. Tunable strongly coupled superconductivity in magic-angle twisted trilayer graphene. *Nature.* 590(7845):249–255.
- 49 Suzuki Y, et al. 2022. Mott-driven BEC–BCS crossover in a doped spin liquid candidate  $\kappa$ -(BEDT-TTF) $_4\text{Hg}_{2.89}\text{Br}_8$ . *Phys Rev X.* 12:011016.
- 50 Zhou P, et al. 2019. Electron pairing in the pseudogap state revealed by shot noise in copper oxide junctions. *Nature.* 572(7770):493–496.
- 51 Božović I, Levy J. 2020. Pre-formed Cooper pairs in copper oxides and  $\text{LaAlO}_3$ – $\text{SrTiO}_3$  heterostructures. *Nat Phys.* 16(7):712–717.
- 52 Bastiaans KM, et al. 2021. Direct evidence for cooper pairing without a spectral gap in a disordered superconductor above  $T_c$ . *Science.* 374(6567):608–611.
- 53 Han X, Liu B, Hu J. 2019. Enhancement of the thermal-transport figure of merit and breakdown of the Wiedemann–Franz law in unitary Fermi gases. *Phys Rev A.* 100:043604.
- 54 Sowiński T, Gajda M, Rzażewski K. 2016. Diffusion in a system of a few distinguishable fermions in a one-dimensional double-well potential. *Europhys Lett.* 113(5):56003.
- 55 Erdmann J, Mistakidis SI, Schmelcher P. 2018. Correlated tunneling dynamics of an ultracold Fermi–Fermi mixture confined in a double well. *Phys Rev A.* 98:053614.
- 56 Griffiths DJ, Schroeter DF. 2018. *Introduction to quantum mechanics.* Cambridge: Cambridge University Press.
- 57 Büttiker M. 1992. Scattering theory of current and intensity noise correlations in conductors and wave guides. *Phys Rev B.* 46:12485–12507.
- 58 Blanter YM, Büttiker M. 2000. Shot noise in mesoscopic conductors. *Phys Rep.* 336(1–2):1–166.
- 59 Imry Y. 2002. *Introduction to mesoscopic physics.* Number 2. Oxford: Oxford University Press on Demand.
- 60 Bouchiat H, Gefen Y, Guéron S, Montambaux G, Dalibard J. 2005. *Nanophysics: coherence and transport: lecture notes of the Les Houches Summer School 2004.* Amsterdam: Elsevier.
- 61 Lumbroso OS, Simine L, Nitzan A, Segal D, Tal O. 2018. Electronic noise due to temperature differences in atomic-scale junctions. *Nature.* 562(7726):240–244.
- 62 Ngampruetikorn V, Parish MM, Levinsen J. 2015. High-temperature limit of the resonant Fermi gas. *Phys Rev A.* 91:013606.
- 63 Zwerger W. 2011. *The BCS–BEC crossover and the unitary Fermi gas.* Vol. 836. Berlin: Springer Science & Business Media.
- 64 Pieri P, Strinati GC. 2000. Strong-coupling limit in the evolution from BCS superconductivity to Bose–Einstein condensation. *Phys Rev B.* 61:15370–15381.
- 65 Andrenacci N, Pieri P, Strinati GC. 2003. Evolution from BCS superconductivity to Bose–Einstein condensation: current correlation function in the broken-symmetry phase. *Phys Rev B.* 68:144507.
- 66 Jarrell M, Gubernatis JE. 1996. Bayesian inference and the analytic continuation of imaginary-time quantum Monte Carlo data. *Phys Rep.* 269(3):133–195.
- 67 Liu XJ. 2013. Virial expansion for a strongly correlated Fermi system and its application to ultracold atomic Fermi gases. *Phys Rep.* 524(2):37–83 (Virial expansion for a strongly correlated Fermi system and its application to ultracold atomic Fermi gases).